Internal Report
DESY F41-76/12
December 1976

Synchrotron Radiation as a Source for Surface Photoemission

by

C. Kunz

Synchrotron Radiation as a Source for Surface Photoemission

C. Kunz

Deutsches Elektronen-Synchrotron DESY, Notkestieg 1, 2000 Hamburg 52, W.Germany

Chapter 17

Table of contents

To be published as Chapter 17 of "Photoemission from Surfaces", Eds. B. Feuerbacher, B. Fitton, and R.F. Willis, John Wiley, London

17.1 Introduction

The availability of a tunable radiation source which covers the spectral range from the visible through the vacuum ultraviolet into the x-ray region opens up a new dimension also for surface studies. Synchrotron radiation from electron synchrotrons and electron (or positron) storage rings is now applied at several laboratories to excite photoelectrons from solids. Since photoemission is always involving the surface of a sample, volume and genuine surface-state properties usually show up in the same experiment. Many of the arguments in favour of a synchrotron radiation source apply equally well to the investigation of bulk and surface properties. One point, however, is of great importance: the possibility to continuously vary the escape depth through a variation of the kinetic energy of electrons which are excited from a specific level is a powerful tool to discriminate between volume and surface states. An escape depth minimum for unscattered electrons as low as one monolayer in thickness occurs for electrons with kinetic energies around 100 eV.

Synchrotron radiation has further advantages, namely the possibility of a variation of the cross section by varying the excitation energy, tuning-in at resonance transitions, and the very useful possibility to have photon energy as a free parameter in angular dependent photoemission. In addition the high degree of polarization can usefully be applied.

Synchrotron radiation is available in principle[1-5] since 1946 but it was considered at that time to be an unwanted by-product of electron acceleration in circular machines, which were installed only for the purposes of nuclear physics. Not before the early sixties a systematic application for spectroscopy in the vacuum ultraviolet (and even later in the x-ray region) began which is reviewed in a series of publications.[6-30] Only

in the last few years programs on surface photoemission were initiated. Now, synchrotron radiation, especially when sources which are built specifically as light sources (so called dedicated storage rings) will become available, is considered to be a powerful tool for surface investigations.

The pace at which this research activity can be expanded is, however, not only determined by the availability of storage rings but also by the set-up and development of an appropriate instrumentation. First of all monochromators with a high efficiency and selectivity are required, further sample chambers with appropriate electron energy analyzers and sample manipulation are necessary.

In section 2 of this chapter the properties and in section 3 the availability of synchrotron radiation are discussed. Section 4 is a survey on the arrangement of experiments in synchrotron radiation laboratories, while section 5 deals with monochromators. In section 6, finally, the different modes in which surface properties can be investigated are discussed. Examples of actual investigations performed with synchrotron radiation are spread over the other chapters of this volume and are not taken into consideration here.

17.2 Properties of Synchrotron Radiation

17.2.1 Calculation of Properties

Synchrotron radiation is emitted by relativistic electrons or positrons when they are deflected in magnetic fields. Consider such particles on circular orbits. In that case one expects radiation at the frequency of revolution because the whole structure is similar to an antenna. The concentration of the charge at discrete points (at short wavelengths all the particles act as independent radiation sources) together with the relativistic velocities lead to a strong enhancement of higher order harmonics. Thus the emitted spectrum can be considered as consisting of a dense continuum extending from the frequency of revolution to very high optical frequencies. Also the high degree of linear polarization in the plane of the synchrotron and the collimation in the instantaneous direction of flight of the electrons follows immediately from the picture of a radiating dipole antenna[5] moving with a relativistic velocity (Fig. 17.1).

The intensity of synchrotron radiation can be calculated from classical electrodynamics. Quantum corrections are negligible for practical purposes. Ivanenko and Pomeranchuk[31] followed by Schwinger[32] were the first to give the theoretical equations. The problem is now dealt with in standard textbooks like those of Sommerfeld[33] and Jackson[34]. We give here the most important final equations of these calculations. While the equations are given for one electron on a circular orbit actual synchrotrons and storage rings contain straight sections between bending magnets. In this case it is better to use the equations for unit particle current which are obtained from the equations as given here by multiplication by $2\pi R/(ec)$, where R is the radius of the orbit (see Fig. 17.2). One important assumption is additivity of the power radiated by several electrons. This only holds if the distribution of electrons around the orbit is random on the scale of the wavelengths emitted. This usually is the case for wavelengths in the optical range, while it does not hold in the microwave range.

Tomboulian and Hartman[5] have transformed the angular distribution of power P to a convenient form:

$$P(\psi,\lambda) = \frac{8}{3}\frac{\pi R e^2 c}{\lambda^4}\gamma^{-4}(1+x^2)^2\left(K^2_{2/3}(\xi) + \frac{x^2}{1+x^2}K^2_{1/3}(\xi)\right), \qquad (17.1)$$

$$x = \gamma\psi, \quad \xi = \left(2\pi R/(3\lambda)\right)\gamma^{-3}(1+x^2)^{3/2}, \quad \gamma = E/(mc^2).$$

Here $P(\psi,\lambda)$ is the power in erg per sec per rad at the azimuth angle ψ relative to the plane of the orbit (see Fig. 17.2) and per unit wavelength interval and λ the wavelength under consideration. E is the energy of the particles and $K_{2/3}(\xi)$ and $K_{1/3}(\xi)$ are modified Bessel functions of the second kind (see e.g. Watson[35]).

Equation (17.1) contains in square brackets two terms. The first one gives the power of radiation with the electric vector oscillating parallel to the plane of the orbit while the second term is the power of the component with the electric vector perpendicular. It follows that in the plane of the orbit the radiation is 100 % linear polarized, while above and below the plane the radiation is right and left hand elliptically polarized since the two components are by $\pm\pi/2$ out of phase. Figure 17.3 shows for an actual example the two different components and the degrees of linear and circular polarization.

When the power according to Eq. (17.1) is integrated over all angles ψ and plotted as a function of wavelength a maximum in the power distribution occurs near a wavelength which is called the critical wavelength λ_c and defined as

or:
$$\lambda_c = \frac{4\pi R}{3}\,\gamma^{-3}\,, \qquad (17.2)$$

or:
$$\lambda_c\,(\text{Å}) = 5.59\ R(m)\cdot\left(E(GeV)\right)^{-3}\,,$$

this corresponds to a critical photon energy

$$\varepsilon_c = 2.22\cdot10^3\ \left(E(GeV)\right)^3\cdot\left(R(m)\right)^{-1}. \qquad (17.3)$$

For applications in solid state spectroscopy respectively surface spectroscopy, a plot of the number of photons available in a constant energy window (e.g. 1 eV) is more useful. Figure 17.4 shows the intensity available into an aperture, which could be accepted by a monochromator at laboratory distance from the tangential point. No maximum occurs any more in such a plot, the critical photon energy ε_c here marks the region where the strong fall-off of the intensity to higher photon energies sets in. Useful intensities are available up to energies $\varepsilon = 4\times\varepsilon_c$. For some experiments, radiation up to photon energies $\varepsilon = 8\times\varepsilon_c$ has been made use of. A good approximation for the number of photons available at photon energies $\varepsilon\ll\varepsilon_c$ (when integrating over all angles) in a horizontal slice, 1 mrad wide, is given by

$$N\left(\frac{\text{photons}}{\text{sec}\cdot\text{eV}\cdot\text{mA}\cdot\text{mrad}}\right) = 4.5\cdot10^{12}\cdot j(mA)\cdot\left(R(m)\right)^{1/3}\cdot\left(\varepsilon(eV)\right)^{-2/3}, \qquad (17.4)$$

with j the current of particles.

17.2.2 Time structure

The time structure of a synchrotron radiation source is determined by the time structure of the particles in orbit. There is time structure in three levels as is shown in Fig. 17.5. The shortest pulse structure, in the order of 100 psec to 1 nsec, is due to the fact that electrons are bunched at stable phase positions on the orbit. At DORIS or DESY 496 such positions are allowed, but not all of them must be filled with particles. The separation of these bunches is 2 nsec. The second type of time structure occurs at the frequency of revolution which at DORIS and DESY is 1 MHz. This is observable since in a synchrotron the filling of the 480 bunches has to have a gap of at least 20 % of the total circumference because of the injection mechanism. At storage rings sometimes only one of the possible

bunches is filled or a gap can also be intentionally inserted into a storage ring filling for purposes of beam stability. The third type of time structure occurs only at synchrotrons and is given by the repetition rate of particle acceleratoin (e.g. 50 Hz).

17.2.3 Comparison with other sources

One of the most important questions which someone who is interested in synchrotron radiation would ask is how it compares in intensity with other sources in the vacuum ultraviolet. The other available continuum and line spectra originate from gas discharge lamps[36,37] some of which are summarized[38] in Fig. 17.6. It is immediately recognized that no single one of these sources can cover a spectral range as large as synchrotron radiation. Further, the peak intensities of the continuum sources are lower by at least one order of magnitude compared to that of a usual synchrotron source, the relative intensities are approximately on scale. The rare gas continua do not overlap and no good source is available below 600 Å. This is a comparison based on actual intensities available on a sample behind the exit slit of a monochromator.

It is difficult to make a direct comparison of the intensities of the sources. Based on the brightness which is the number of photons emitted by a source per unit area per unit solid angle such a comparison could be given.[39] The maximum brightness of a synchrotron radiation source which is an angle dependent brightness with its peak value in the plane of the orbit is by several orders of magnitude higher than the brightness of gas discharge sources. A properly designed monochromator set-up could, however, collect a fairly large solid angle from the classical source which usually

is not feasible with a synchrotron radiation source. Another difficulty in making a comparison usually has its origin in the fact that many different designs of discharge lamps are in existence but only a few investigators really bother to give quantitative figures on the output of these lamps.

The He I resonance line at 21.2 eV photon energy should be mentioned separately. This line has a width of <20 meV and can be used without a monochromator. One figure quoted[40] for its intensity is 5.10^{11} photons on the sample. This high intensity is by about two orders of magnitude larger than what is available from a synchrotron together with a monochromator and still somewhat higher than obtainable at one of the presently operating storage ring laboratories. It is possible, however, to surpass the intensity of the He I line with a dedicated storage ring source and an appropriate monochromator.

At wavelengths below 600 Å soft x-ray tubes are available but their intensity is too low for photoemission spectroscopy. Further the BRV-source[41] which consists of a spark discharge with uranium rod electrodes has been used for absorption spectroscopy. This source, however, is pulsed and not useful for photoemission spectroscopy. In the x-ray region synchrotron radiation cannot really compete in intensity with characteristic lines from x-ray tubes, again because of solid angle considerations. With big dedicated x-ray storage rings the situation will alter, since then there will be sufficient intensity. The special qualities of synchrotron radiation, like tunability, polarization, and the possibility to obtain high monochromatization with the parallel beam and plane crystal monochromators will make also this spectral region attractive.

17.3 Presently Available and Future Synchrotrons and Storage Rings

There are presently three cathegories into which synchrotron radiation sources can be classified.

1. Parasytically used synchrotrons,
2. parasitically used storage rings,
3. storage rings, dedicated to synchrotron radiation work.

A wide variety exists also in the extent to which these instruments are used for synchrotron radiation experiments. Table 17.1 lists more than twenty synchrotrons and storage rings which are of interest in this context. The main problem with the cathegories 1. and 2. is that the conditions of operation of these machines are determined by the needs of high energy physics. There are several points giving rise to collision of interests:

1. Beam energy. This according to Eq. (17.3) determines the high energy cut-off of the spectrum.
2. Beam current. A high energy counter experiment may want a reduction of current while highest current is usually wanted by spectroscopists. At storage rings high energy physicists optimize "luminosity"+) which does not automatically require the highest possible current.
3. Complexity. A single stored beam in a storage ring is much easier to handle than two colliding beams.
4. Planning ahead. Machine conditions are usually not planned for a long period in advance, since planning depends on the recent results of the high energy experiments.
5. Design parameters. In a storage ring for particle physics the design is determined by obtaining optimum beam conditions at the interaction point of electrons and positrons. As a synchrotron radiation source such a machine should have its smallest beam size in the bending magnets.

+) "Luminosity" is the ratio of the number of electron-positron collisions divided by the cross section.

In general the VUV experiments are usually better served than the x-ray experiments, which do not get light at all if the energy is not high enough according to Eq. (17.3). Also there are a few smaller storage rings now operated as light sources only. These, however, were, with the exception of the one in Tokyo,[42,43] not conceived as such from the outset. Of all these storage rings the one at Stoughton[44] is definitely the most successful one. Even as a near VUV source its energy, however, is too low.

There is now a world-wide interest in building storage rings which are planned as sources of radiation from the beginning. There are two types of dedicated storage rings under consideration.[25,26] One would be a small machine with about 700 MeV energy and a critical energy ε_c of about 500 eV. This machine would serve the VUV range only, but for this range it would be more useful than any of the big machines. Such a small machine provides only VUV radiation on the first optical elements. Therefore they can take a greater load of useful radiation without deterioration or damage. Further, such small machines allow for a small distance between source and experiment which results in the collection of a much wider horizontal angle of the radiation pattern. This will result in much larger intensity on a sample e.g. in a photoemission experiment. Also the beam lines do not require a large investment. In addition, the small machine gives the advantage that experimenters can work right at the experimental chamber while the beam is on without danger of radiation hazards if radiation safety is considered already in the design stage of the machine.

A large x-ray machine needs at least 2 - 3 GeV. To build such a storage ring is already a major untertaking in which a large group of accelerator physicists and engineers are involved. NINA II is one of these projects which presently is in the stage of construction.[45] Other proposed projects of this kind are the Brookhaven storage ring, the Photon Factory project

in Japan and TANTALUS 2.5. The main design effort with these storage rings would concentrate on making the beam as small as possible.

In addition, the proposals for these projects also contain the option of inserting multipole wigglers[46-48] into straight sections of the beam. A low radius bend in the beam could push the short wavelength limit of such a storage ring further down. A multipole wiggler, due to a interference effect, would yield a spike in the spectrum at a wavelength:

$$\lambda \approx \frac{\lambda_\omega}{\gamma^2} \qquad (17.5)$$

where λ_ω is the periodicy wavelength of the wiggler. For λ_ω = 9 cm, $\gamma = 3 \cdot 10^3$ ($\triangleq$ 1.5 GeV), $\lambda \approx 100$ Å follows. These devices, however, have not yet been tested at storage rings. Before they really can go into operation they would need probably a serious test phase. If these wigglers really work, a storage ring equipped with them could probably be called already a 4. cathegory machine in continuation of the classification given above.

17.4 Arrangement of Experiments

While the installation of experiments at smaller storage rings, like TANTALUS I is fairly simple and quite straight-forward[44] (beam lines are short, access to the experiment is given during operation, adjustment of the optical components can be done making use of the visible part of synchrotron radiation), the use of large scale machines poses special problems. Fig. 17.7 shows the arrangement of beams at the storage ring laboratory[49] at DORIS. Some details and the considerations which led to this arrangement will be explained.

The synchrotron radiation laboratory has a distance from the tangential point between 31 and 44 m. A reduction of that distance by about 10 m would have been possible at the price of a considerable increase in building and shielding costs. The beam transport to the laboratory is determined by radiation safety and vacuum considerations. Further, the highest possible power of about 100 Watt/mrad, when the storage ring runs at maximum current, necessitates the installation of a movable water cooled absorber A to protect valves V when they are closed.

The radiation safety requires several collimators around the beam pipe in the tunnel, a lead beam-shutter BS and a permanent bending magnet M which would deflect charged particles which might eventually be lost during injection or from the stored beam. Since injection of electrons is the most dangerous mode, the beam shutter cannot be opened when injection occurs. This is no real disadvantage because stable conditions as a light source exist only with a stored beam. At energies up to 3 GeV the x-ray part of the spectrum is weak enough to be shielded by the stainless steel beam pipes. If no x-ray window is installed the only hazards can arise from a unwanted loss of one filling. This necessitates to prevent access of personell to a region 40 cm around the direct beam D in the laboratory. The deflected beams L_1, L_2 and R_1 are accessible.

The vacuum of a storage ring has to be in the 10^{-10} range in order to reduce collisions of the stored beam with rest gas molecules. Further, any hydrocarbons are unwanted since they lead to carbon layers on the insulators in the microwave cavities. At the same time these hydrocarbons are cracked on the optical components especially on the first deflecting mirrors where the flux is high. Therefore it is quite necessary to preserve the ultra-high vacuum in the whole beam-line system. Only sample chambers which are

buffered by an ultra-high vacuum monochromator may have higher pressures if necessary. Therefore the whole beam line system and the monochromators are designed for pressures below 10^{-9} Torr. Further a fast-closing valve FCV protects the storage ring in case of vacuum break-down at the experiments.

A beam of 3.8 mrad horizontal width is brought into the labcratory and is split into 3-4 individual beams by grazing incidence mirrors. These plane mirrors are made of a glass-ceramic material "zerodur" (Schott and Gen., Mainz) with no surface coating. Contamination or heating have not caused any serious problems up to now but contamination definitely does occur.

Installations at the other big laboratory connected to a high-energy storage ring, SPEAR,[48,50] are quite similar to those at DORIS. There again monochromators in deflected beams are accessible during operation while the x-ray beams are shielded. Each x-ray experiment is individually protected by a pair of beam stoppers and a shielded hutch. These are individually accessible when the beam stoppers are closed. The primary beam is only accessible if the main beam shutter is closed. The typical distance of the experimental stations at SPEAR from the source point is 20 m. In this case the first deflecting mirrors are made of polished copper blocks which are kept automatically at a constant temperature.[51]

17.5 Monochromators

The monochromators which are of interest for surface photoemission spectroscopy are instruments which deliver a high flux of photons in the energy range 10 - 1000 eV onto the spot of samples determined by the aperture of the electron analyzer. Different instruments are used for different

spectral regions within this range.[52] In principle one can distinguish between normal incidence monochromators, which cover the energy range 5 - 40 eV and grazing incidence instruments which cover the range beyond 40 eV.

There are several near-normal incidence monochromators commercially available which are described in the book by Samson.[37] These instruments have fixed entrance and exit slits. In order to be optimally matched to the synchrotron radiation source the monochromators should disperse in a vertical plane. In this case the source image fits better to the horizontal slits and the s polarized reflectance from the grating is higher than the otherwise p polarized reflectance. This is of special importance with a Seya monochromator the transmissivity of which is strongly dependent on the direction of polarization. Since the ordinary commercial instruments are dispersing horizontally, changes have to be asked for from the manufacturer. The entrance slit is best illuminated with a doubly focusing premirror in order to match the source to the acceptance of the monochromator. Grazing incidence torroidal mirrors can be used.[53]

A near-normal incidence Wadsworth type monochromator was especially invented by Skibowski and Steinmann[54] for the geometry found at large synchrotrons or storage rings. It is an intermediate resolution instrument which uses the source as the entrance slit. Fig. 17.8 shows the design principle. The almost parallel light falls on the grating which focuses the radiation onto the exit slit. The grating is rotated around an excentric point. The excentric arrangement guarantees a good approximation to the focusing condition over a wide wavelength range. Although this is a very simple instrument it has the disadvantage that its resolution cannot be improved beyond a certain limit since the source size is given. Typically 1 Å

resolution is reached with a 1200 lines/mm grating.

Eastman et al.[55] used very successfully a combination of a commercial Seya and an simple grazing incidence monochromator to cover the range 5 - 120 eV in one sample chamber for photoemission studies. The disadvantage of this instrument is that the grazing incidence monochromator is not capable of continuous scanning.

Grazing incidence monochromators which deliver a fixed exit beam are commercially not available. Only the knowledge of the performance of reflecting elements which was continuously growing over the years of research with synchrotron radiation allowed for the realization of fairly complex instruments with several optical elements which fulfil this requirement.[52] Figs. 17.9 and 17.10 show the principle of two of them which are successfully in operation, the Grashopper[56] at SPEAR and the FLIPPER[57] at DORIS.

The Grashopper[56] consist of a focusing premirror M_1 which moves along the beam together with the entrance slit S_1. The entrance slit is of the type first used by Codling et al.[58]. It consist of a combination of a mirror and a single jaw slit. The second jaw is the image of the first one in the mirror. Such a slit can reflect the incoming light always onto the grating by rotating the mirror-slit combination. The slit S_1 the grating and the exit slit S_2 are constrained to move on the Rowland circle. This results in a fixed exit beam. This monochromator operates in the range from about 40 to 500 eV. As usual with a Rowland instrument (at fixed slit width) the energy resolution interval is proportional to the square of the photon energy. Another problem with this instrument is the overlap of several spectral orders with contributions depending on the individual properties of the grating used.

The FLIPPER[57] is a UHV adaption of a predecessor instrument[59] which is successfully in operation now for many years at the DESY synchrotron. The principle of operation is shown in Fig. 17.10. One of six different plane mirrors M_1-M_6 reflect the incoming radiation at grazing angles of incidence between 4° and 50° onto a plane grating. The plane grating disperses the incoming radiation one wavelength of which is then focused by a paraboloidal mirror onto the exit slit. The wavelength is varied by rotating the grating. This instrument has many options. By choosing an appropriate mirror for each photon energy higher order radiation can be rejected. In addition each mirror has two different optical coatings. By sliding the mirror further in or out they can be interchanged. If higher order rejection is not needed high resolution at long wavelengths can be achieved by using a mirror with a fairly grazing angle which increases the dispersion. This instrument has shown excellent performance in its first tests.

Energy analyzers[60] used for surface photoemission work will not be described here. It should be mentioned, however, that the double pass cylindrical mirror analyzer is by far the most popular one. Its angular acceptance lies on a cone. For angular dependent photoemission measurements a small section of this cone can be selected by an added diaphragm. Other possible choices are plane mirror analyzers or spherical condensor analyzers. The spot size on the sample at which these analyzers are sensitive usually is in the order of 1 mm^2.

17.6 Techniques of Surface Photoemission

17.6.1 Energy distribution curves (EDC)

The usual way to measure photoemission with classical line sources is to measure energy distribution curves (EDC). This technique is of course also

one of the methods used in connection with synchrotron radiation. In this case a series of different EDC spectra can be obtained with different photon energies[61] at arbitrary energy spacing. This allows e.g. for a variation of matrix elements. The different matrix elements for different shells in rare gas atoms[61], are plotted in Fig. 17.11. These are also representative for different shells in other atoms (and also for solids). In addition to the matrix element considerations the mean free path can be varied by varying the kinetic energy of the electrons[62], which is shown schematically in Fig. 17.12. This is of course of considerable importance for surface physics because it allows for a variation of the relative intensity ratio of surface to volume structures and thus for an identification of surface states. Finally, the variation of the direction of polarization with respect to the plane of incidence (s- and p-polarization) and with respect to bond directions of adsorbates is feasible with synchrotron radiation for all photon energies. This opens up the possibilities to study surface barrier induced states and the orientation of adsorbates as was mentioned already in previous chapters.

17.6.2 Yield spectroscopy

There are further techniques which can only be applied when a continuum source is available. One of them is yield spectroscopy. In yield spectroscopy all the electrons excited at a certain photon energy are collected on a detector while the photon energy is scanned. It can be shown theoretically (see chapter 2) and it was proved in a number of experiments[63-66] that in the regime of core level excitations the yield is proportional to the absorption coefficient which is representative for the topmost several layers of the sample. If surface states or adsorbates are present these also contribute to the total yield with their respective absorption coefficient.

The following somewhat simplified considerations[63] should serve to explain yield spectroscopy. The total photoelectric yield has three contributions as visualized in Fig. 17.13: primary excitation, Auger electrons from the decay of the hole state, and direct recombination (autoionization). These electrons usually have a considerable kinetic energy and therefore according to Figs. 17.12 and 17.13 undergo electron-electron scattering. This scattering is accompanied by electron multiplication. From the electron distribution which results from these processes those electrons, which have kinetic energies a few eV above the vacuum level, have the largest mean free path and therefore the highest chance to escape from the solid. Their mean free path, which is in the order of 50 Å for metals can be very large for insulators as it is indicated in Fig. 17.12. (In this region, where electron-electron interband scattering is not possible many-phonon and impurity scattering are the escape length determining factors.) These consideration lead to the following equation for the yield $Y(\omega)$

$$Y(\omega) \propto F(\omega) \cdot \mu(\omega) \cdot D \qquad (17.6)$$

where D is an average escape depth, $\mu(\omega)$ the absorption coefficient and $F(\omega)$ a multiplication factor. Here $\mu(\omega) \cdot D$ is proportional to the number of photons absorbed in the sensitive layer of thickness D. $F(\omega)$ is approximately proportional to $\hbar\omega$. The reason is the following: if we put e.g. an energy of $\hbar\omega$ = 70 eV into the surface layer after multiplication this could result in 10 electrons of 7 eV each, while a photon of $\hbar\omega$ = 140 eV gives rise to 20 electrons at 7 eV. Of course, only part of these electrons will have a chance to escape and the problem needs a statistical treatment.

Equation (17.6) shows that all the fine-structure in $Y(\omega)$ will have its origin in the structure of $\mu(\omega)$. This was demonstrated in a series of experiments[63-67] and was already exploited for the investigation of structures in the absorption coefficient of liquid metals[68] and single crystals.[63]

Because of the surface sensitivity of this method transitions from core levels to empty surface states could also be investigated by this method.[69] Historically the first systematic investigations of the similarity of photoelectric yield and the absorption coefficient was made by Lukirskii and coworkers[64] in the soft x-ray region with the bremstrahlungs continuum of x-ray tubes.

17.6.3 Partial yield spectroscopy and constant final state spectroscopy (CFS)

The surface sensitivity of yield spectroscopy can be varied by selecting only those scattered electrons which fall into a certain energy interval. As long as scattered electrons with a photon energy independent energy distribution are selected this partial yield is still proportional to the total yield. When, however, electrons of increasing kinetic energy are selected the escape depth is reduced (see Fig. 17.12) and surface state contributions to the yield are enhanced. This was first demonstrated by Eastman and Freeouf.[69] The method is called partial yield spectroscopy.

The same type of spectroscopy is also called constant finnal state spectroscopy (CFS) in investigations with a different scientific goal.[70] In this case the aim was not the investigation of structure in the absorption behavior of a solid but the investigation of the primary excited electrons. This is visualized in Fig. 17.14. In fixing a kinetic energy of the electrons a final state energy E^{o}_{kin} is fixed. When scanning the photon energies electrons from the occupied levels are excited to the final states at the energy E. Thus the spectra resemble EDC curves but with different weight-functions which are determined by different matrix elements.

These spectra are usually interpreted within the framework of one-electron interband transitions using constant matrix elements but they are useful even when this model breaks down. The number of photoelectrons excited into an energy interval around the kinetic energy E is given by[61]

$$N(E,\hbar\omega) \propto \int d^3\underset{\sim}{k}\, M_{if}(\underset{\sim}{k})\ \delta(E_f(\underset{\sim}{k})-E_i(\underset{\sim}{k})-\hbar\omega)\ \delta(E_f(\underset{\sim}{k})-E) \qquad (17.7)$$

with i, f initial and final states, $\underset{\sim}{k}$ the vector in the reciprocal lattice, E_i, E_f initial and final state energies, $M_{if}(\underset{\sim}{k})$ the matrix element for dipole transitions between the filled band i and the empty band f at the point $\underset{\sim}{k}$ in the Brillouin zone. When making the assumption (which by no means is easy to justify even in simple cases) that the value of $M_{if}(\underset{\sim}{k})$ has a negligible variation with $\underset{\sim}{k}$, we can take M in front of the integral and write

$$N(E,\hbar\omega) \propto M(E,\hbar\omega)\cdot\rho_i(E-\hbar\omega)\cdot\rho_f(E) \qquad (17.8)$$

where ρ_i and ρ_f are the initial and final state densities. In constant final state spectroscopy (CFS) the influence of the variation of ρ_f on the spectra is elminiated. If further, $M(E,\hbar\omega)$ can be set constant altogether CFS probes $\rho_i(E-\hbar\omega)$, the density of occupied states.

17.6.4 Constant initial state spectroscopy (CIS)

There is another kind of spectroscopy, which can be used with a continuum light source. It is called constant initial state spectroscopy[70-72] (CIS) and can be explained from Eq. (17.8) and Fig. 17.15. In this case $E - \hbar\omega = E_{const.}$ which is achieved by making a synchronous scan of the light monochromator and the electron analyzer. $\rho_i(E_{const.})$ is fixed by this method and all the excitations from one given filled level to different empty levels are registered. Under the simplifying assumption that $M(E,\hbar\omega)$ = const. such a spectrum provides a picture of the density of unoccupied levels $\rho_f(E)$.

17.6.5 Investigation of primary and secondary processes by EDC, CFS, and CIS

In summarizing and comparing the three types of spectroscopy on the basis of a one-electron density of states model they can be characterized in the following way:

1. EDC (variaton of E) measures a joint density of states,
2. CFS (variation of $\hbar\omega$) measures the density of occupied (initial) states,
3. CIS (variation of $E-\hbar\omega$) measures the density of unoccupied (final) states.

The interpretation does not depend on the fact that $\underset{\sim}{k}$ in Eq. (17.7) has the meaning of a vector of the reciprocal lattice. An equation completely analogous to (17.8) holds for photoemission from surface and adsorbate states.

Actually the latter two types of spectroscopies help to investigate the deviation from the density of states (DOS) approach. In each of the three cases there is one free parameter. In CFS this parameter for instance is the final state energy. A series of spectra in the DOS approximation should have an identical shape. The same should hold for a series of CIS spectra as a function of the initial state energy. In reality these series of spectra show differences and shifts of oscillator strength. There the limitation of the DOS approximation show up and can be investigated.

Further, the whole picture, as it was explained above, is only taking into consideration those electrons which originate from primary excitations. But there is a background of scattered electrons underlying the structured features. The Auger peaks will appear in CFS spectra at the corresponding Auger energies. In CIS spectra the Auger peaks show up for those initial states from which the Auger electrons are ejected.[70] In EDC spectra Auger electrons occur always at fixed Auger energies while the direct excitations move in a series of EDC spectra with $\hbar\omega$.

Direct recombination of resonance states deriving from deep levels (autoionization) accompanied by an excitation from the valence band is best proved from CIS spectra.[70] While scanning through the resonance a strong feature should appear.

17.6.5 Angular dependent CFS

There are special advantages for surface state spectroscopy in combining these spectroscopies with angular dependent photoemission. One of the attractive possibilities which should be of special value in the investigation of metals is the selection of a final state energy which falls in a band gap. When integrating over the whole Brillouin zone the different conduction bands overlap in such a way that no gap in the density of final states occurs. When, however, a final state energy E and a spatial direction are fixed this determines a straight line parallel to the surface normal in k space. The bands along such a line can have gaps and if properly chosen the final state energy lies in such a gap. In this case the photoemission from volume states is considerably reduced while the emission from occupied surface states will dominate.

17.6.7 Conclusion

The enrichment of surface state and adsorbate photoemission due to the availability of a continuum source like synchrotron radiation should have become evident in this chapter. In summarizing, two new types of electron spectroscopy in addition to the traditional EDC's namely CFS and CIS become feasible. Yield spectroscopy is very simple and can be understood as an integrated CFS spectroscopy. Further, the possibility to reach directional energy gaps in the final states in metals (and insulators) is very promising. Resonances, like localized surface excitations and surface excitons, become accessible objects of investigation.[73] Moreover, there is the possibility to vary volume and surface sensitivities by taking advantage of the varying mean free path

of an excited electron with photon energy. Finally, the varying matrix elements can be exploited for gaining optimum sensitivity for the excitation from different shells and for the identification of adsorbate states by comparing the intensity variation of peaks in EDC spectra in the adsorbed and free adsorbate atoms or molecules.[74]

Acknowledgment

The author is grateful to W. Gudat and E.E. Koch for a critical reading and to Mrs. E. Thumann for her careful typing of this manuscript.

References

1. J.P. Blewett, Phys.Rev. 69, 87 (1946)
2. F.R. Elder, A.M. Gurewitsch, R.V. Langmuir, and H.C. Pollock, Phys.Rev. 71, 829 (1947) and J.Appl. Phys. 18, 810 (1947)
3. P.L. Hartman and D.H. Tomboulian, Phys.Rev. 87, 233 (1952)
4. P.L. Hartman and D.H. Tomboulian, Phys.Rev. 91, 1577 (1953)
5. D.H. Tomboulian and P.L. Hartman, Phys.Rev. 102, 1423 (1956)
6. R. Haensel and C. Kunz, Z.Angew. Physik 23, 276 (1967)
7. A.A. Sokolov and J.M. Ternov "Synchrotron Radiation" translated from the Russian, Pergamon Press, Oxford (1968)
8. R.P. Godwin, Springer Tracts in Modern Physics 51, 1 (1969)
9. G. Rosenbaum and K.C. Holmes, Nature 230, 434 (1971)
10. W. Hayes, Contemp.Phys. 13, 441 (1972)
11. G.V. Marr, I.M. Munro and J.C.C. Sharp, Synchrotron Radiation: A Bibliography, Daresbury, Nuclear Physics Laboratory, Report DNPL/R24 (1972) and DL/TM127 (1974)
12. G.V. Marr and I.M. Munro eds., Proc. Intern. Symposium for Synchrotron Radiation Users, Daresbury, Nuclear Physics Laboratory, Report DNPL/R26 (1973)
13. R.E. Watson and M.L. Perlman, Brookhaven National Laboratory, Report BNL 50 381 (1973)
14. K. Colding, Rep.Progr.Phys. 36, 541 (1973)
15. F.C. Brown, Solid State Physics 29, 1 (1974)
16. E.E. Koch, R. Haensel and C. Kunz eds. "Vacuum Ultraviolet Radiation Physics", Vieweg-Pergamon, Braunschweig (1974)
17. E.E. Koch in: Chemical Spectroscopy and Photochemistry in the VUV eds.: C. Sandorfy, P.J. Ausloos and M.B. Robin, Reidel, Dodrecht, 1974, p. 559
18. M.L. Perlman, E.M. Rowe, and R.E. Watson, Physics Today 27, 30 (July 1974)
19. R.P. Madden in: X-Ray Spectroscopy, Ed. L.V. Azároff, McGraw-Hill, New York 1974. p. 338

20. J. Taylor, in: Chemical Spectroscopy and Photochemistry in the Vacuum Ultraviolet. Eds.: C. Sandorfy, P.J. Ausloos, and M.B. Robin, Reidel, Dodrecht (1974) p. 543

21. R. Haensel in: Festkörperprobleme, Advances in Solid State Physics, Vol. 15, Ed.: H.J. Queisser, Pergamon-Vieweg, Braunschweig (1975), p. 203

22. E.E. Koch, C. Kunz and B. Sonntag, Physics Report 1976, to be published

23. B. Sonntag, in "Rare Gas Solids II", eds. M.L. Klein and J.A. Venables, Academic Press, New York (1976) in press

24. C. Kunz, in "Optical Properties of Solids , - New Developments" ed. B.O. Seraphin, North-Holland, Amsterdam-New York (1976) p. 473

25. "An Assessment of the National Need for Facilities Dedicated to the Production of Synchrotron Radiation", Report to the National Academy of Sciences, Washington D.C. 1976

26. J.Wm. McGowan and E.M. Rowe eds., Proceedings of Synchrotron Radiation Facilities, Quebec Summer Workshop, Report University of Western Ontario, London, Ontario 1976

27. C. Kunz, Phys.Bl. 32, 9 (1976) and 32, 55 (1976)

28. J. Barrington Leigh and G. Rosenbaum, Anual Review of Biophysics and Bioengineering 5, 239 (1976)

29. E.E.Koch in: "Interaction of Radiation with Condensed Matter", L.A. Self ed. , publ. of the Trieste Center for Theor. Physics, Int. Atom. Energy Agency, Wien 1976

30. G. Zimmerer in: Proceedings of the Intern. Summer School on Synchrotron Radiation Research. Alghero 1976, I.C.A.P. Series, Vol. 5, I.F. Quercia Ed., Catania, 1976

31. D. Ivanenko and J. Pomeranchuk, Phys.Rev. 65, 343 (1944)

32. J. Schwinger, Phys.Rev. 70, 798 (1946) , Phys.Rev. 75, 1912 (1949)

33. A. Sommerfeld, "Elektrodynamik", Akademische Verlagsgesellschaft, Leipzig (1949)

34. J.D. Jackson, "Classical Electrodynamics", Wiley, New York (1962), p. 481 ff

35. G.N. Watson, Bessel Functions, McMillan, New York 1945, p. 188

36. Y. Tanaka, A.S. Jursa and F.J. LeBlank, J.Opt.Soc.Am. 48, 304 (1958)

37. J.A.R. Samson, Techniques of Vacuum Ultraviolet Spectroscopy, J. Wiley, New York (1967)

38. E.E. Koch, Proc. 8th All Union Conf. of High Energy Particle Physics, Erevan. April 1975, Vol. 2, Erevan (1976), p. 502

39. C. Kunz in Ref. 16, p. 753

40. J.A. Kinsinger, W.L. Stebbings, R.A. Valenzi and J.W. Taylor in: Electron Spectroscopy, Ed. D.A. Shirley, North-Holland, Amsterdam 1972, p. 155

41. G. Balloffet, J. Romand, and B. Vodar, C.R. Acad.Sci. (Paris) 252, 4139 (1961) and H. Damany, G. Mehlman and J. Romand, in Ref. 16, p. 720

42. T. Miyahara, H. Kitamura, T. Katayama, M. Watanabe, S. Sato, E. Ishiguro, M. Endo, Sh. Yamaguchi, T. Yamakawa, Se. Yamaguchi, and T. Sasaki, Report, Institute of Nuclear Studies, Tokyo INS-TH-107, June 1976

43. H. Kitamura, T. Miyahara, S. Sato, M. Watanabe, S. Mitani, E. Ishiguro, T. Fukushima, T. Ishii, Sh. Yamaguchi, M. Endo, Y. Iguchi, H. Tsujikawa, T. Sugiura, T. Yamakawa, Se. Yamaguchi and T. Sasaki, Report, Institute, of Nuclear Studies, Tokyo, INS-TH-108

44. E.M. Rowe and F.E. Mills, Particle Accelerators 4, 221 (1973)

45. Daresbury Nuclear Laboratory, Report DL/SFR/R2 (1975)

46. B. Kincaid, J.Appl.Phys. to be published

47. J.P. Blewett and R. Chasman, J.Appl.Phys. to be published

48. K.O. Hodgson, H. Winick, and G. Chu, Eds. Synchrotron Radiation Research, SSRP Report No. 76/100, August 1976

49. E.E. Koch, C. Kunz, and E.W. Weiner, Optik 45, 395 (1976)

50. H. Winick in Ref. 16, p. 776

51. J.L. Stanford, V. Rehn, D.S. Kyser, V.O. Jones, and A. Klugman in Ref. 16 p. 783

52. C. Kunz in Ref. 12, p. 68

53. V. Saile, P. Gürtler, E.E. Koch, A. Kozevnikov, M. Skibowski and W. Steinmann, Appl. Optics 15, 2559 (1976)

54. M. Skibowski and W. Steinmann, J.Opt.Soc.Am. 57, 112 (1967)

55. D.E. Eastman, W.D. Grobman, J.L. Freeouf and M. Erbudak, Phys.Rev. B9, 3473 (1974)

56. F.C. Brown, R.Z. Bachrach, S.B.M. Hagström, N. Lien and C.H. Pruett, in Ref. 16, p. 785

57. W. Eberhardt, G. Kalkoffen and C. Kunz, to be published

58. K. Codling and P. Mitchell, J.Phys. E.: Sci.Instrum. 3, 685 (1970)

59. H. Dietrich and C. Kunz, Rev.Sci.Instrum. 43, 434 (1972)

60. K.D. Sevier, Low Electron Energy Spectrometry, Wiley, New York 1972

61. see e.g. D.E. Eastman, in Ref. 16, p. 417

62. see e.g. I. Lindau and W.E. Spicer, J. Electron Spectroscopy 3, 409 (1974)

63. W. Gudat and C. Kunz, Phys.Rev.Lett. 29, 169 (1972)

64. A.P. Lukirskii and I.A. Brytov, Fiz. Tverd. Tela 6, 43 (1964) [Sov. Phys. - Solid State 6, 32 (1964)]; A.P. Lukirskii and T.M. Zimkina, Izv. Akad. Nauk SSSR, Ser.Fiz. 28, 765 (1964); A.P. Lukirskii, O.A. Ershov, T.M. Zimina and E.P. Savinov, Fiz.Tverd. Tela 8, 1787 (1966) [Sov.Phys. - Solid State 8, 1422 (1966)]

65. W. Gudat and C. Kunz, Proc.Int.Symp. "X-ray spectra and electronic structure of matter", München 1972, Eds. A. Faessler and G. Wiech, Vol. I, p. 131

66. W. Gudat, Thesis University Hamburg 1974, Internal Report DESY F41-74/10

67. W. Gudat, C. Kunz and H. Petersen, Phys.Rev.Lett. 32, 1370 (1974)

68. H. Petersen and C. Kunz, Phys.Rev.Lett. 35, 863 (1975)

69. D.E. Eastman and J.L. Freeouf, Phys.Rev.Lett. 33, 1601 (1974)

70. G.J. Lapeyre, Solid State Commun. 15, 1601 (1974)

71. G.J. Lapeyre, Phys.Rev.Lett. 33, 1290 (1974)

72. G.J. Lapeyre, J. Anderson, J.A. Knapp, and P.L. Gobby, in Ref. 16, p. 380

73. G.J. Lapeyre and J. Anderson, Phys.Rev.Lett. 35, 117 (1975)

74. T. Gutstafsson, E.W. Plummer, D.E. Eastman and J.L. Freeouf, Solid State Commun. 17, 391 (1975)

75. D.J. Kennedy and S.T. Manson, Phys.Rev. A5, 227 (1972)

Table 1 Synchrotrons (SY) or storage rings (ST) used (or considered) as light sources. E, particle energy; R, magnet radius; I, max current (during acceleration for SY); ε_c, characteristic photon energy; "Exp. Stations" gives only an approximate number of experimental stations, if no number is given we lack information on this point.

Name and location	Type	E(GeV)	R(m)	I(mA)	ε_c(eV)	Exp. Stations	Remarks
Group I, ε_c = 1- 60 eV							
Tantalus I (Stoughton)	ST	.24	.64	100	48	10	dedicated
Surf II (Washington)	ST	.24	.83	∿30	37	5	dedicated
INS-SOR II (Tokyo)	ST	.3	1.1	∿50	54	(∿7)	dedicated
Group II, ε_c = 60 - 2000 eV							
Bonn I (Bonn)	SY	.5	1.7	30	163	3	SR Lab
ACO (Orsay)	ST	.55	1.11	35	333	∿5	dedicated
C-60 (Moscow)	SY	.68	2	10	349		
Aladdin (Stoughton)	ST	.75	2.08	1000	450		proposed, ded.
Frascati (Frascati)	SY	1.1	3.6	15	821	2	
PACHRA (Moscow)	ST	1.3	4	100	1220		dedicated SR Lab
Adone (Frascati)	ST	1,5	5.0	60	1550	(1)	SR Lab
Group III, ε_c = 2 - 30 keV							
Brookhaven (Upton)	ST	2.0	∿8	1000	2200		proposed ded.
Nina II (Daresbury)	ST	2.0	5.55	1000	3200		dedicated under construction
DCI (Orsay)	ST	1.8	3.82	400	3390	4	SR Lab
Tantalus 2.5 (Stoughton)	ST	2.5	6.95	1000	5000		proposed, ded.
Phot.Fac (Japan)	ST	2.5	8		4300		proposed, ded.
Bonn II (Bonn)	SY	2.5	7.65	30	4530	4	SR Lab
Vepp 3 (Novosibirsk)	ST	2.5	6.15	∿100	5600		SR Lab
DORIS (Hamburg)	ST	3.5	12.12	500	7850	8	2 SR Labs
SPEAR (Stanford)	ST	4	12.7	60	11200	∿8	SR Lab
NINA I (Daresbury)	SY	5.0	20.8	50	13300	8	SR Lab
ARUS (Erevan)	SY	6.0	24.65	20	19500	3	SR Lab
DESY (Hamburg)	SY	7.5	31.7	30	25500	10	2 SR Labs
Group IV, $\varepsilon_c \geq$ 30 keV							
Cornell III (Ithaca)	SY	12	120	2	32000	1	SR Lab
Pep (Stanford)	ST	15	170	100	44000		under construction
Petra (Hamburg)	ST	19	200	90	75000		under construction

Figure captions

Fig. 17.1 Angular intensity distribution of slow (a) and relativistic (b) electrons on a circular orbit. The dipole pattern (a) is greatly distorted (b) into the forward direction of the electron because of the relativistic transformation. (From Tomboulian and Hartman[5]).

Fig. 17.2 Intensity distribution around the orbit of the electron. ψ is the angle of emission relative to the plane of the orbit. (From Ref. 38).

Fig. 17.3 Angular distribution of intensity components with electrical vector parallel ($I_{\parallel}$) and perpendicular ($I_{\perp}$) to the plane of the electron orbit. ψ is the angle relative to this plane. Linear polarization and circular polarization (from decomposition into left and right hand circular polarized intensities (I_L and I_R) are also given. (From Ref. 24).

Fig. 17.4 Spectral distribution in an aperture 1 mrad x 1 mrad around the tangential point for DESY and DORIS at different conditions of operation. The characteristic energies ε_c are marked by open circles. (From Ref. 49).

Fig. 17.5 Time structure of synchrotron radiation emission at different levels of time scale expansion. (From Ref. 38).

Fig. 17.6 Schematic comparison of spectral distribution of synchrotron radiation from a synchrotron at different acceleration energies with the continua emitted by several discharge lamps (after Ref. 36). The intensities are roughly on scale. (From Ref. 38).

Fig. 17.7 Layout of the synchrotron radiation laboratory at DORIS. Shown is a section of the storage ring, the beam line to the laboratory and the location of different experiments in the laboratory. For details see text. (From Ref. 49).

Fig. 17.8 Near-normal incidence Wadsworth type monochromator of Skibowski and Steinmann[54]. (From Ref. 54).

Fig. 17.9 Grashopper grazing incidence monochromator by Brown et al.[56] at SPEAR. The scanning of wavelength is visualized by showing two positions corresponding to wavelength λ and zero order. M_1 = focusing premirror, S_1 mirror entrance slit assembly, G = grating, S_2 = exit slit. (From Ref. 56).

Fig. 17.10 FLIPPER grazing incidence monochromator by Eberhardt et al.[57] at DORIS. Only one of the plane mirrors M_1 - M_6 reflects radiation at a time onto the grating, G = plane grating, FM = focusing paraboloid mirror, S = exit slit.

Fig. 17.11 Calculated photoemission cross sections for the photoionization cross sections of outer shell electrons after Kennedy and Manson[75]. (From Ref. 61).

Fig. 17.12 Typical mean free path of electrons with different kinetic energies in metals and insulators (schematic). For insulators an electron-electron scattering threshold at 7 eV is assumed.

Fig. 17.13 Contribution of primary and secondary processes to the EDC photoemission spectrum (schematic). As an example the density of states DOS (a) of an insulator is assumed with one filled core band and the valence band. (b) primary excitation by photons of energy $\hbar\omega$, c) electron-electron scattering after the primary excitation process, d) Auger decay of a core hole, e) direct recombination of a core exciton (autoionization). E_B = binding energy, E_{ex} = exciton energy, E_{vac} = vacuum level, E_{kin} = kinetic energy of the electrons.

Fig. 17.14 Constant final state spectra (CFS) visualized as generated from a series of EDC spectra at different photon energies $\hbar\omega$. The energy interval ΔE_{kin} at the energy E^{o}_{kin} is kept fixed, $\hbar\omega$ is varied. Thus the initial states are scanned.

Fig. 17.15 Constant initial state spectra (CIS) visualized as generated from a series of EDC spectra at different photon energies $\hbar\omega$. The interval which accepts the electrons with kinetic energy E_{kin} is shifted synchronously with $\hbar\omega$. Thus the final states are scanned.

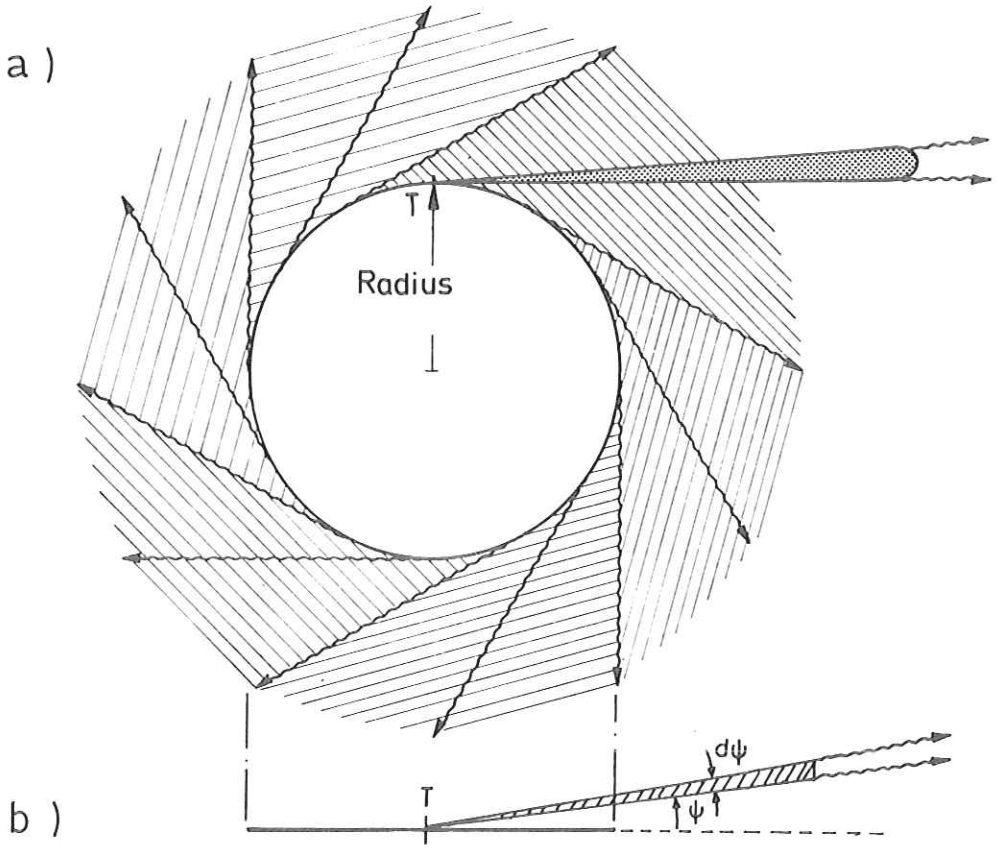

Fig. 17.2

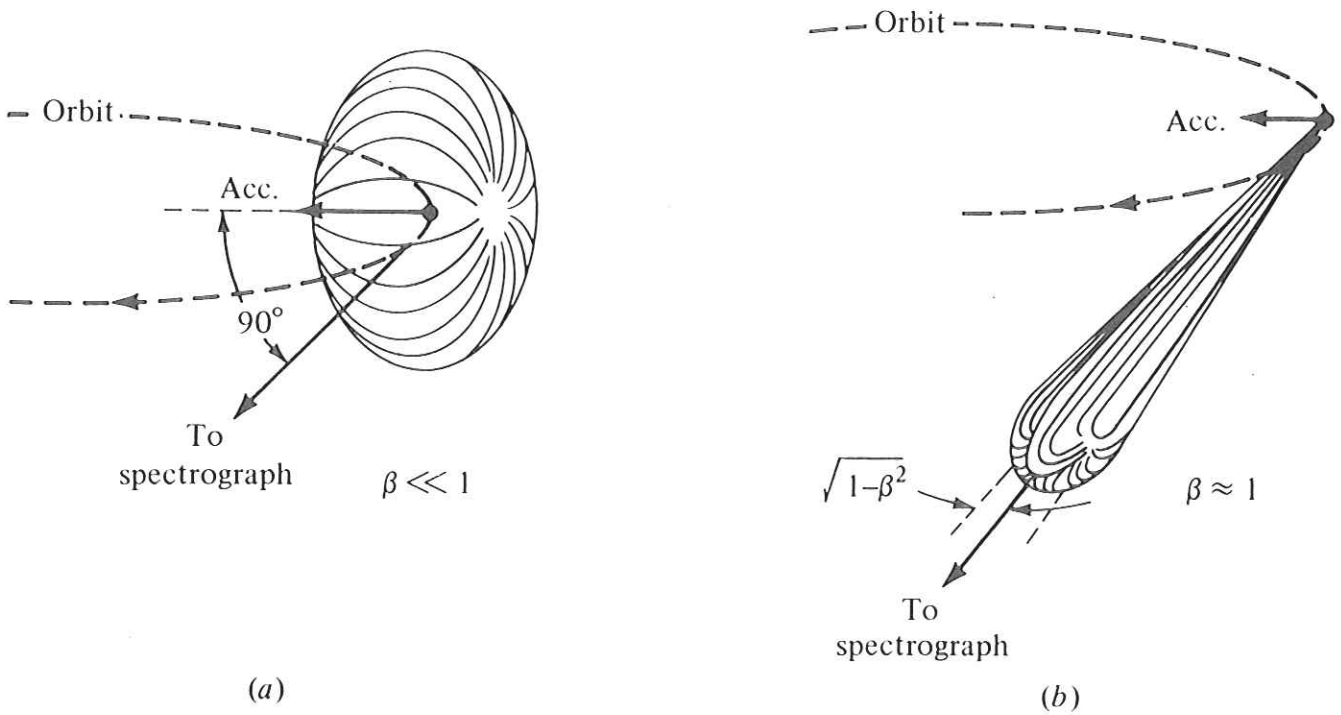

Fig. 17.1

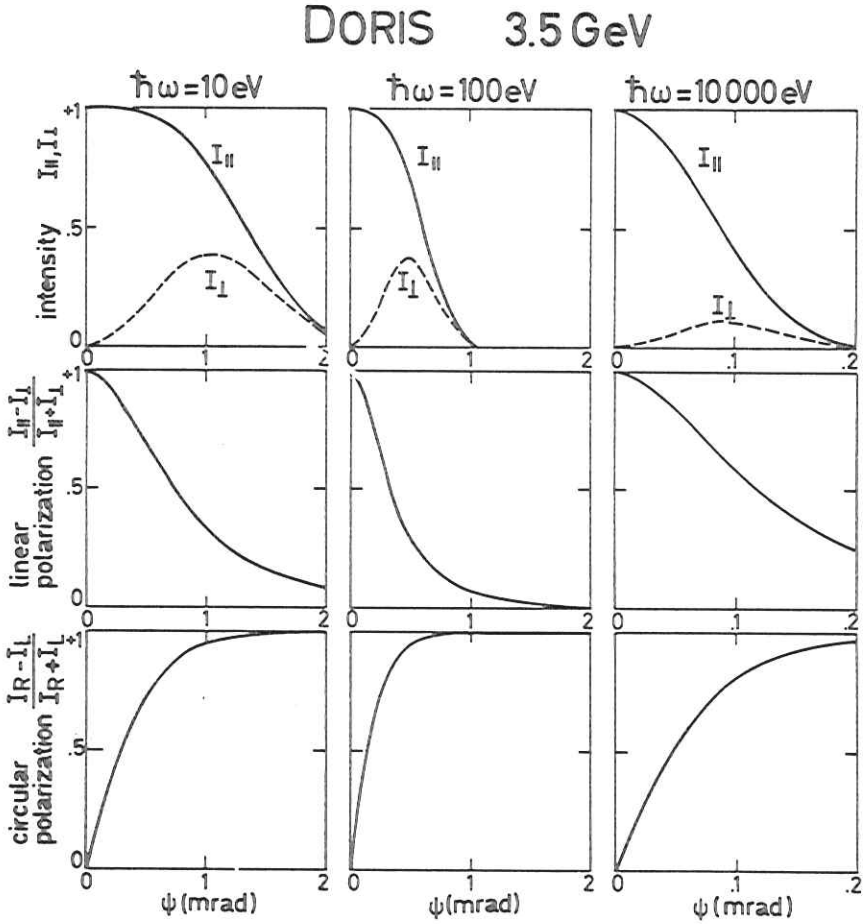

Fig. 17.3

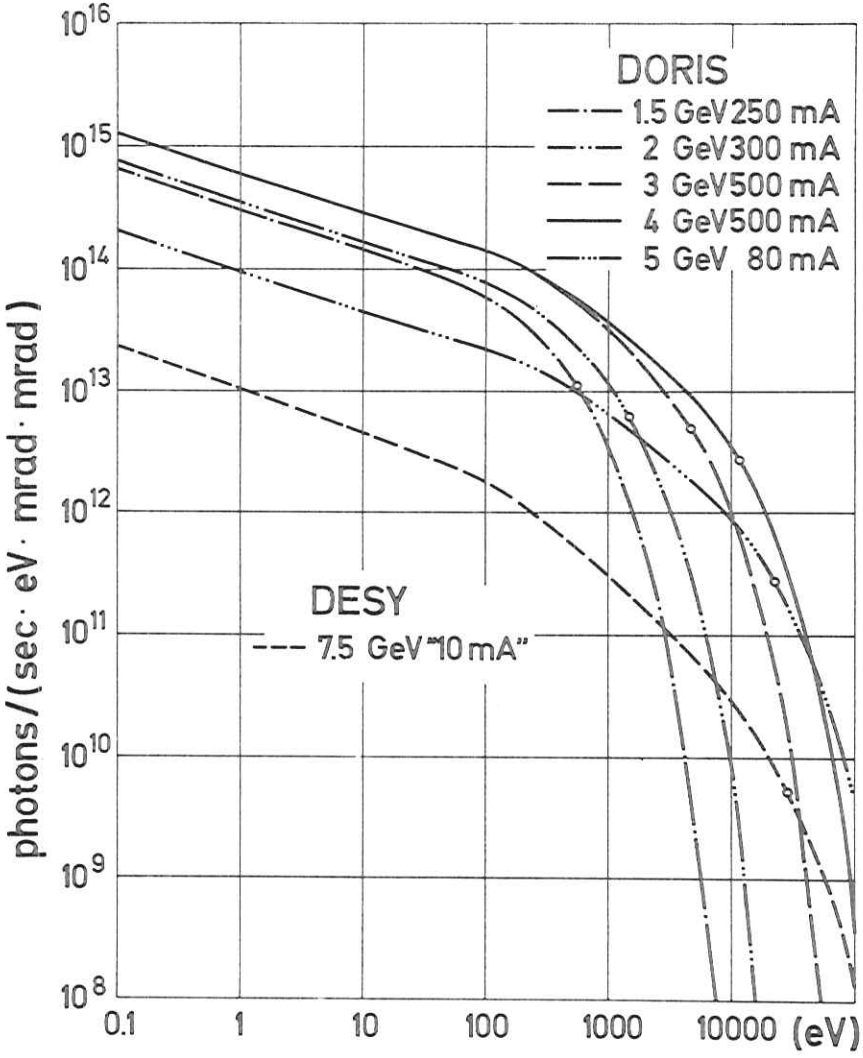

Fig. 17.4

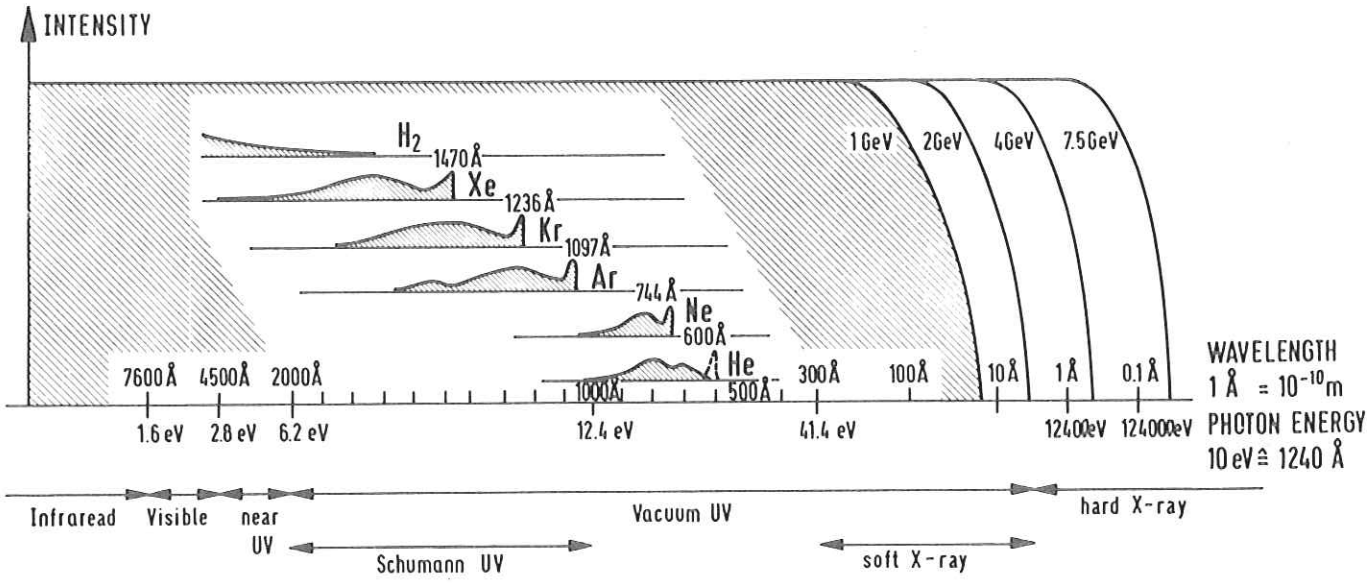

Fig. 17.6

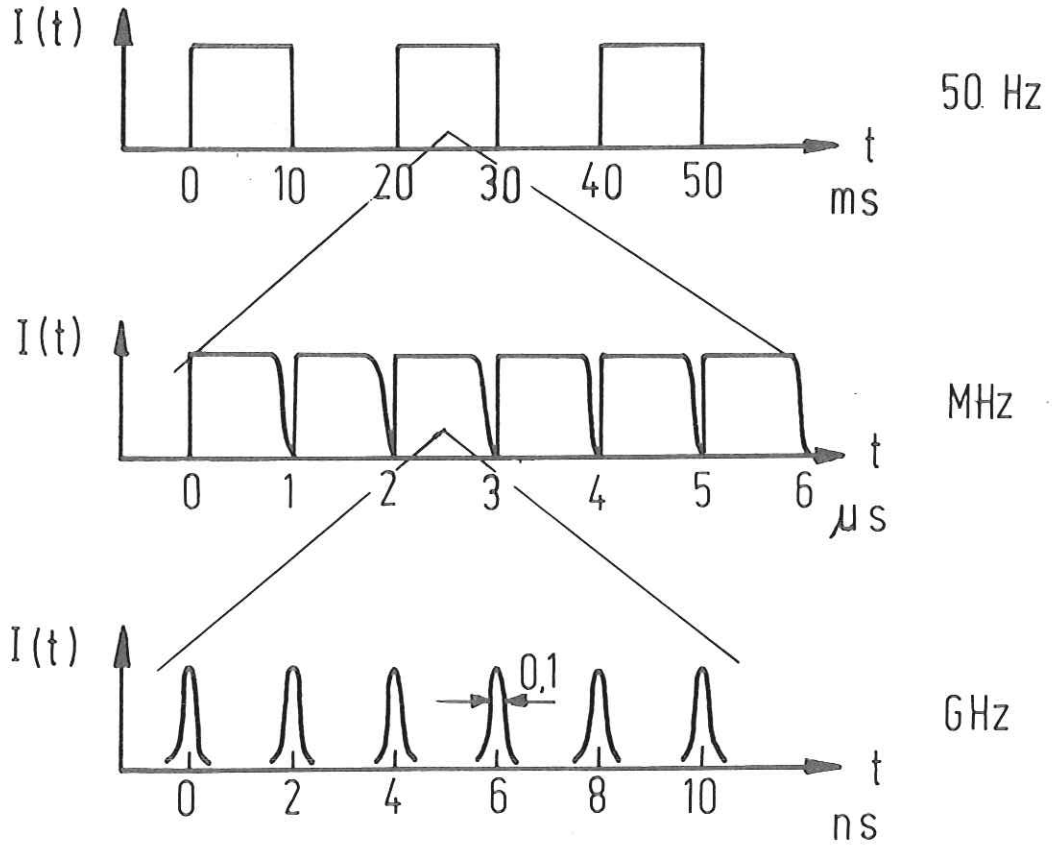

Fig. 17.5

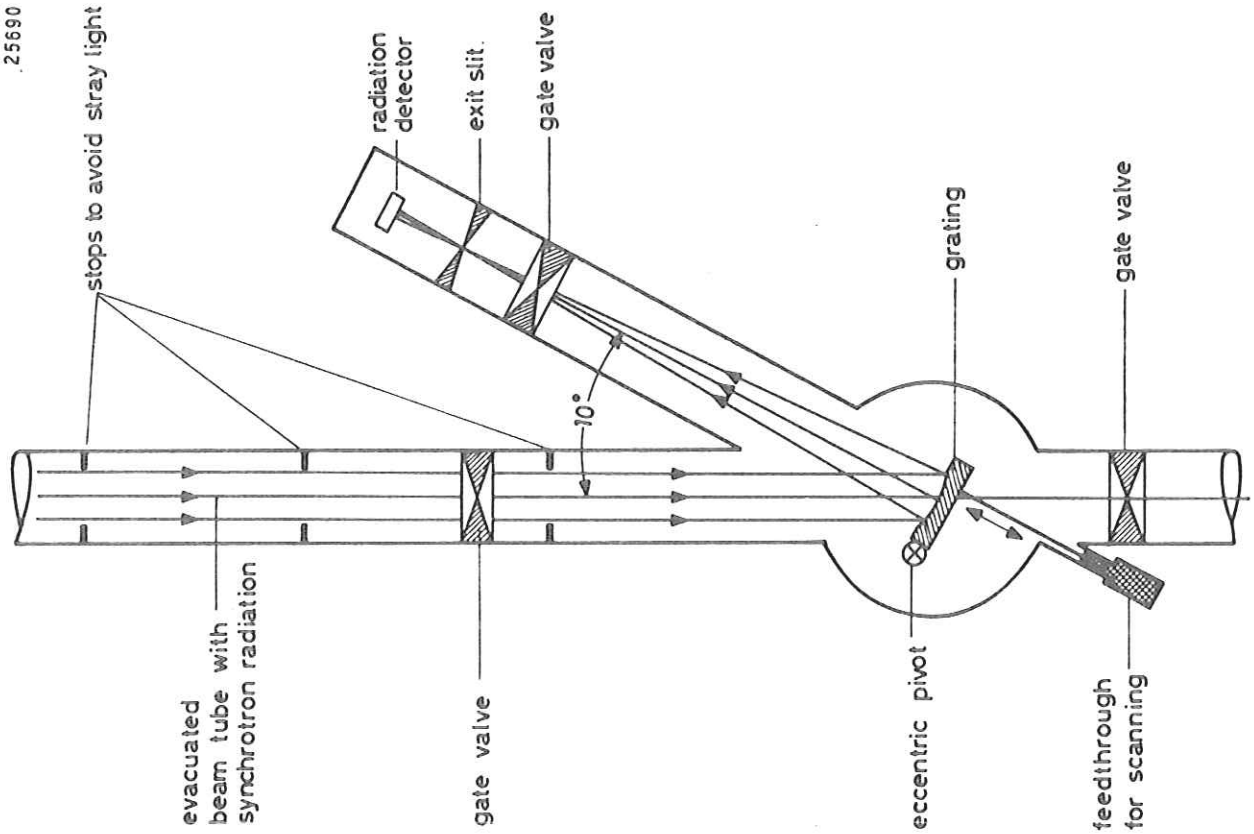

Fig. 17.8

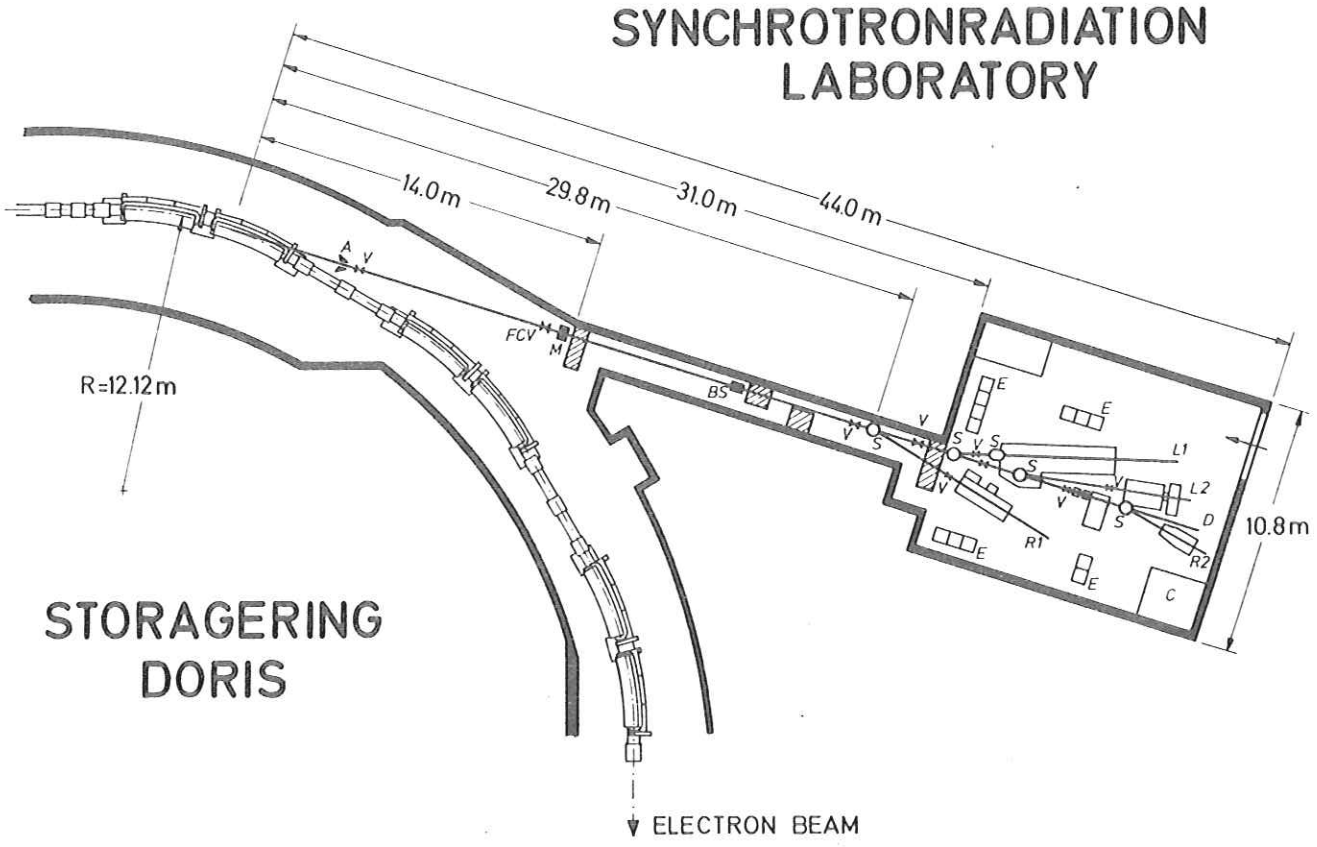

Fig. 17.7

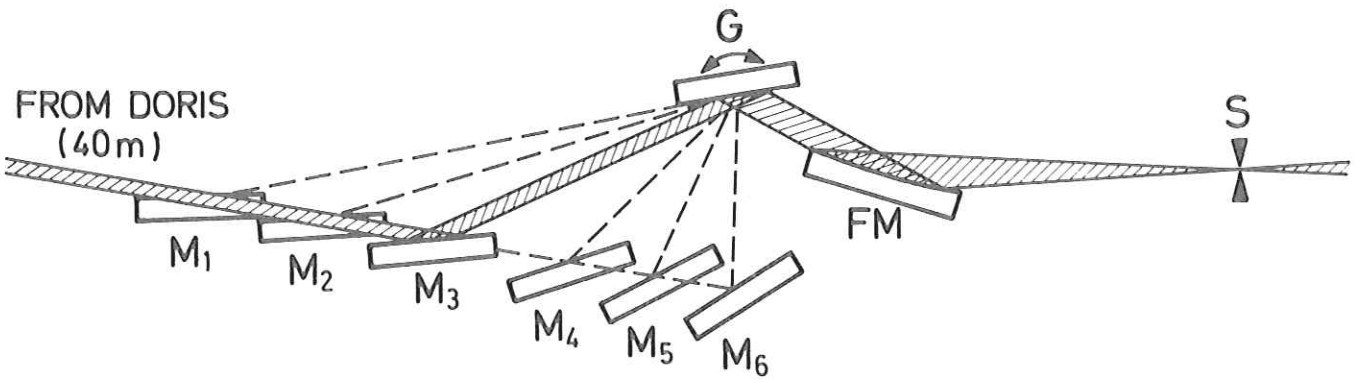

Fig. 17.10

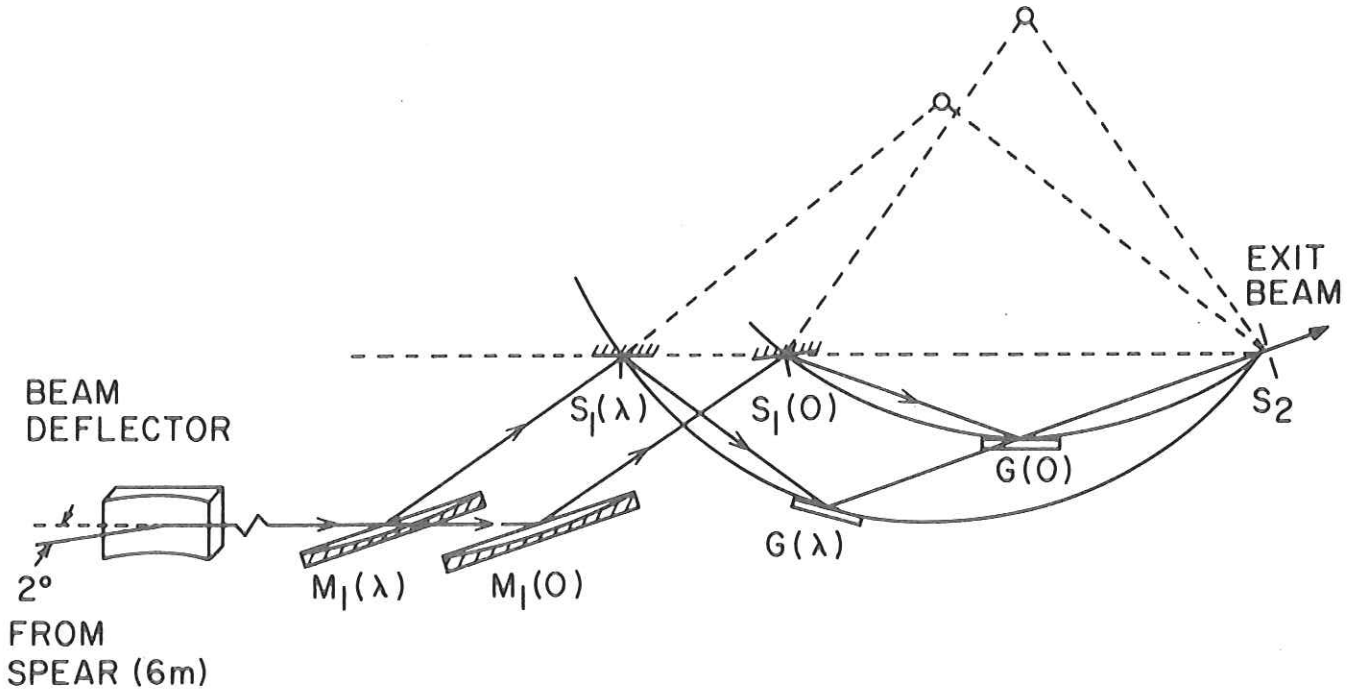

Fig. 17.9

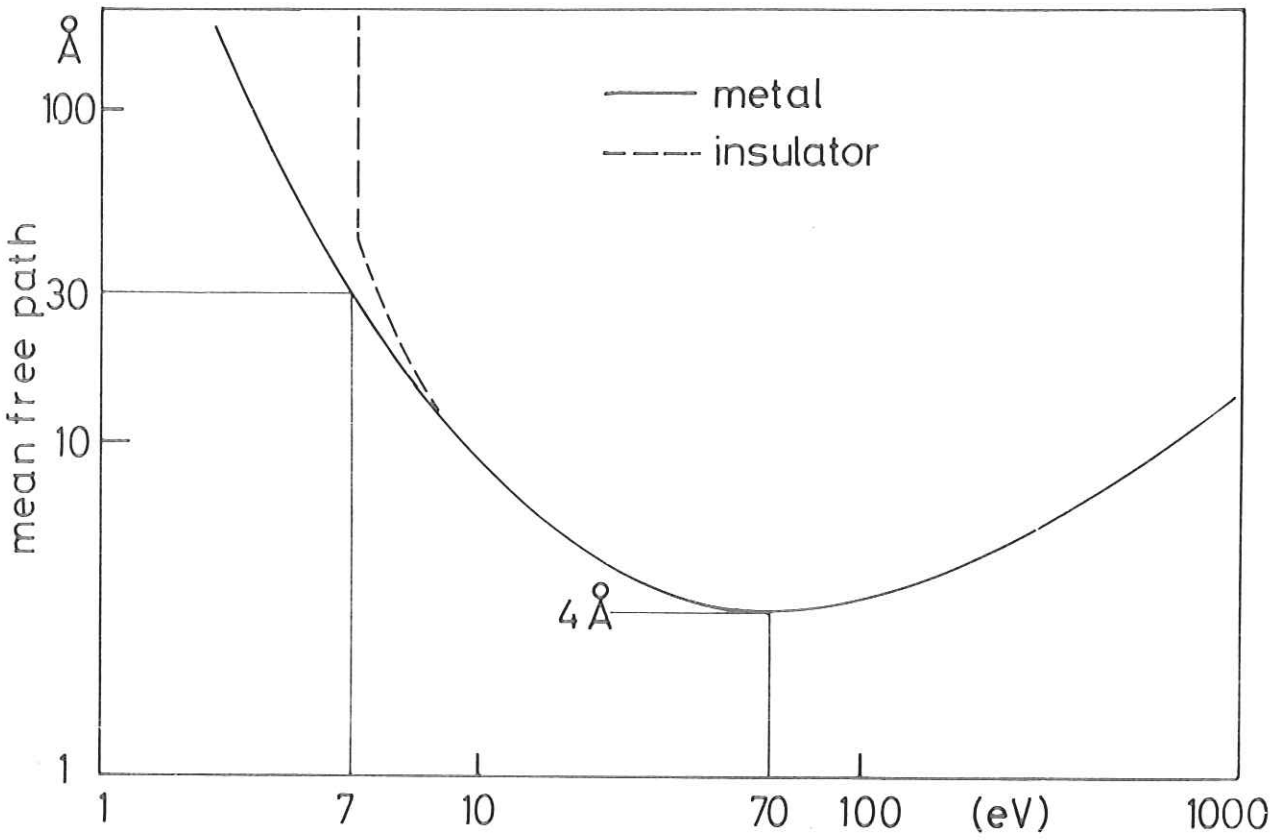

Fig. 17.12

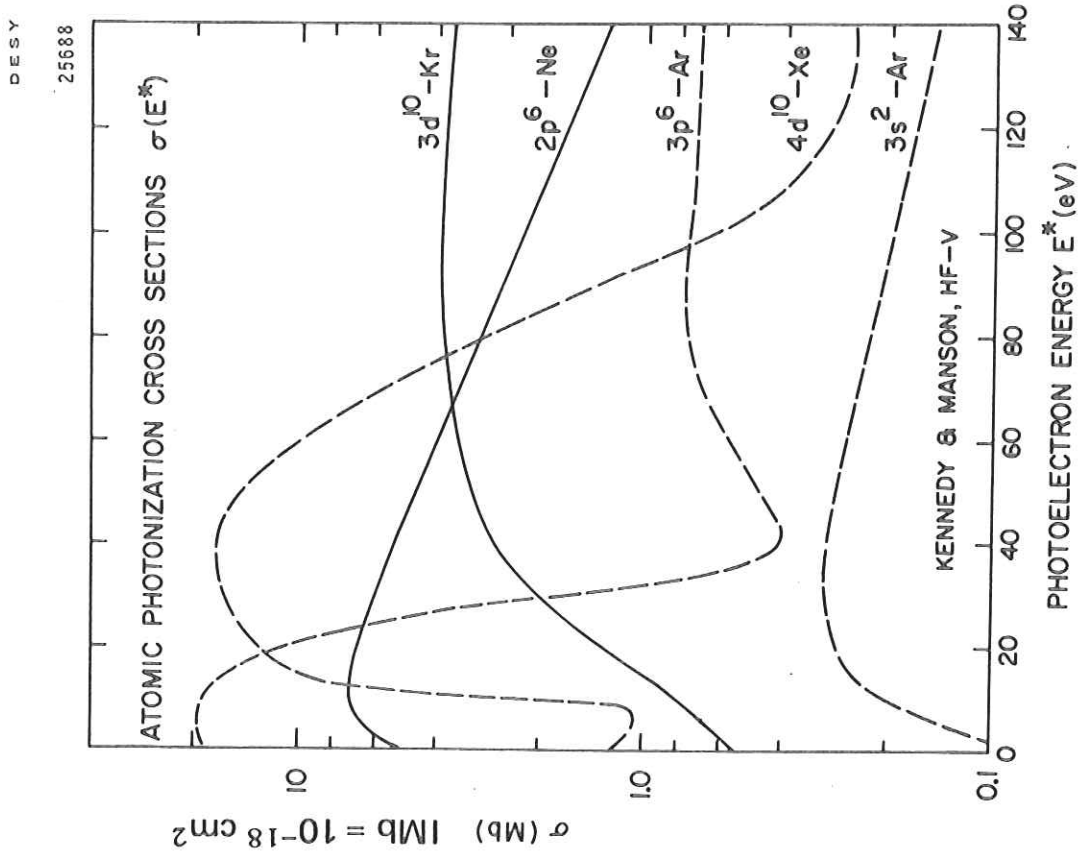

Fig. 17.11

DESY

25702

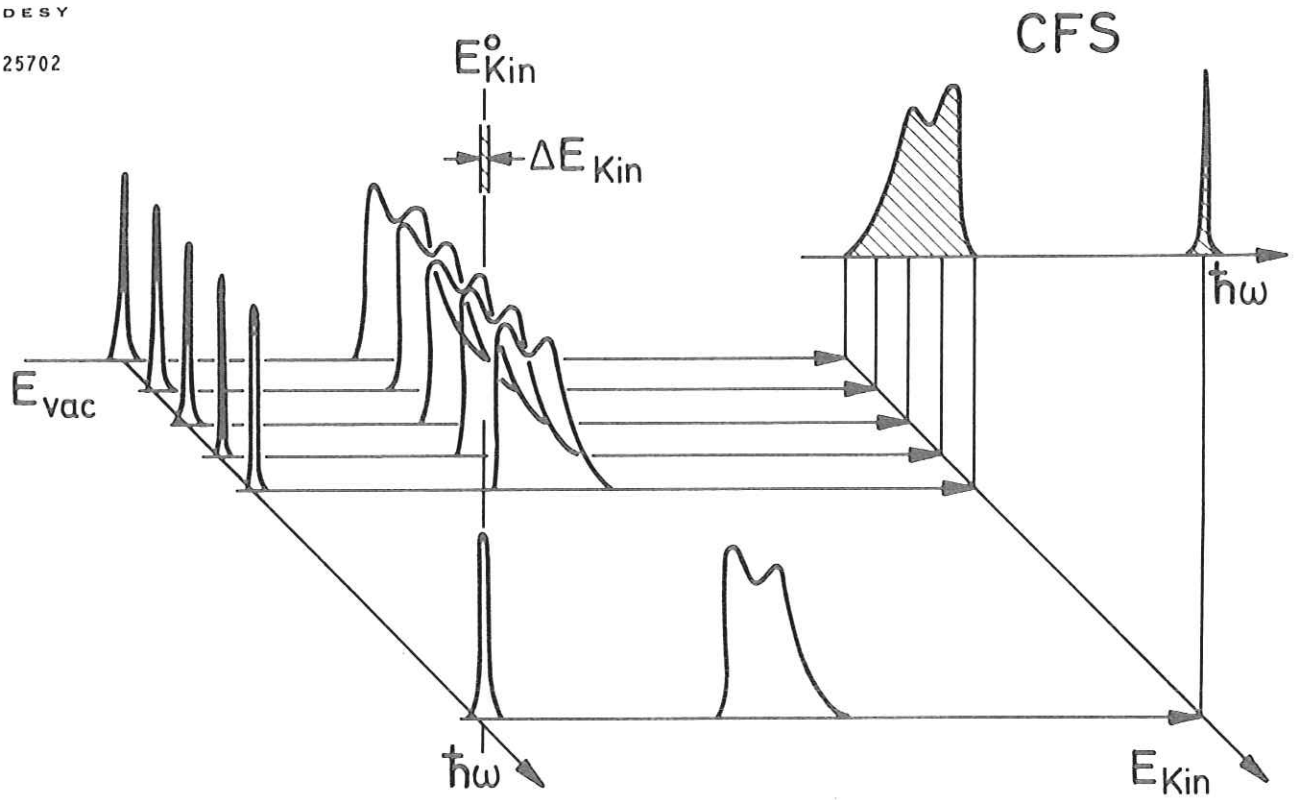

Fig. 17.14

DESY

25703

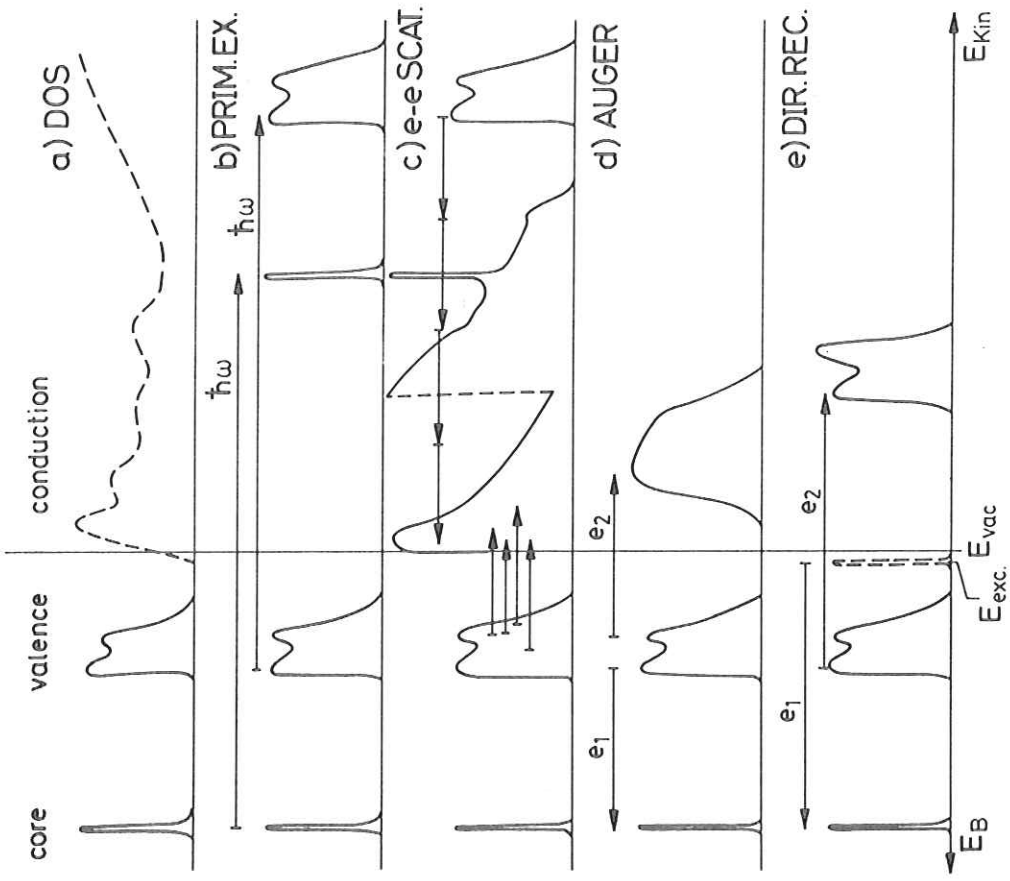

Fig. 17.13

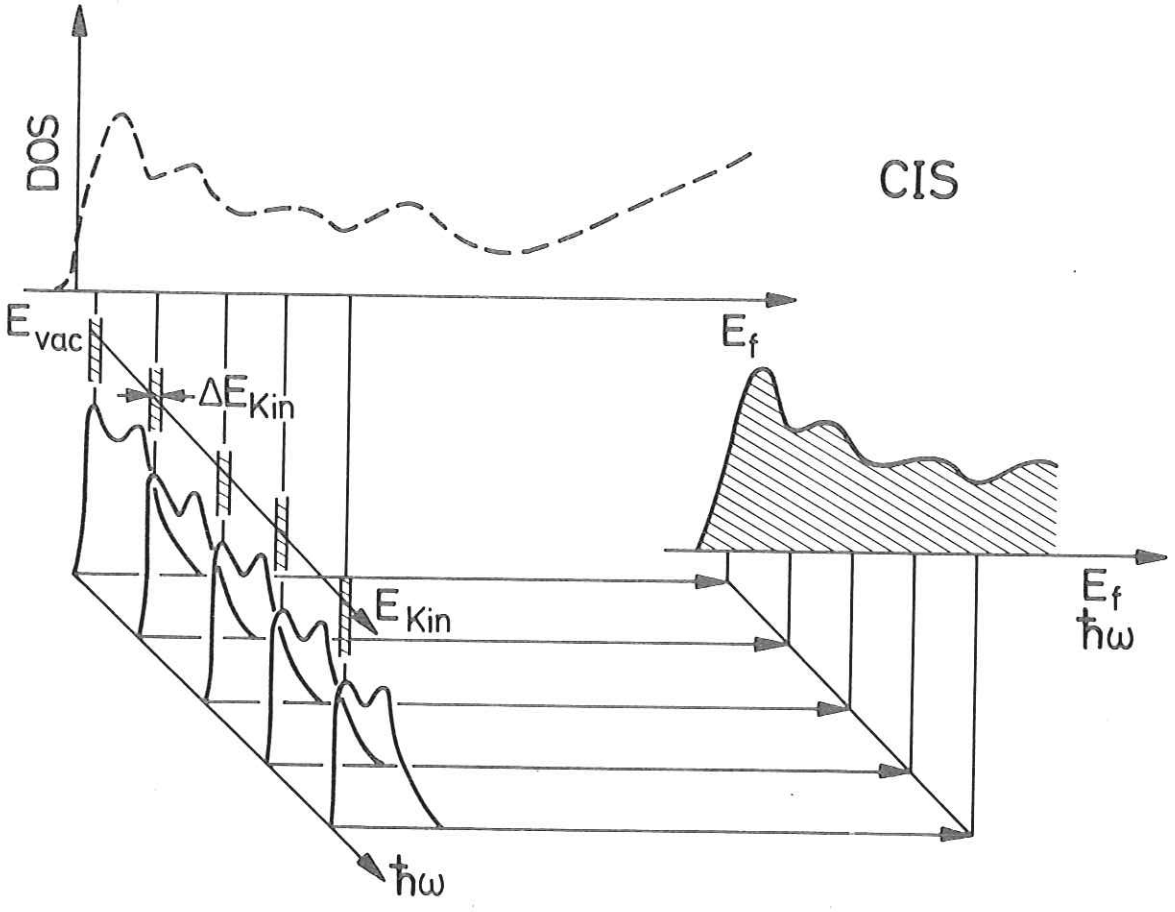

Fig. 17.15